Investigating the mechanism of [M-H] + ion formation in photoionized N-alkyl-substituted thieno [3, 4-c]-pyrrole-4, 6-dione derivatives during higher-order MS n high-resolution mass spectrometry

Salim Sioud, Maan Amad, Zhiyong Zhu, Denis Lesage, Héloïse Dossmann

Investigating the mechanism of $[M–H]^+$ ion formation in photoionized *N*-alkyl-substituted thieno [3, 4-c]-pyrrole-4, 6-dione derivatives during higher-order MS^n high-resolution mass spectrometry

Salim Sioud[*1], Maan Amad[1], Zhiyong Zhu[2], Denis Lesage[3], Héloïse Dossmann[3]

[1] Analytical Chemistry Core Laboratory, King Abdullah University of Science & Technology, Saudi Arabia

[2] KAUST Supercomputing Laboratory, King Abdullah University of Science & Technology, Saudi Arabia

[2] Sorbonne Université, CNRS, Institut Parisien de Chimie Moléculaire, IPCM, F-75005 Paris, France

ABSTRACT

Rationale

The mechanism underlying dopant-assisted APPI's formation of ions is unclear and still under debate for many chemical classes. In this study, we reexamined the gas-phase reaction mechanisms responsible for the generation of $[M–H]^+$ precursor ions, resulting from the loss of a single hydrogen atom, in a series of *N*-alkyl-substituted thieno[3,4-c]-pyrrole-4,6-dione (TPD) derivatives.

Methods

Atmospheric pressure photoionization along with higher-order MS/MS^n using high-resolution mass spectrometry (APPI-HR-CID-MS^n) and electronic structures calculations using density functional theory were used to determine the chemical structure of observed $[M–H]^+$ ions.

Results

As a result, the higher-order MS^n (n=3) experiments revealed a reversed-Diels-Alder fragmentation cleavage mechanism leading to a common fragment ion at *m/z* 322 from the studied

$[M_{1\text{-}5}–H]^+$ ion species. In addition, the calculation for two chemical structure models (*N*-alkyl-TPD1 and *N*-alkyl-TPD5) revealed that the fragment structure by removing the H atom connected to the 3rd carbon atom of the *N*-Alkyl side chain has a more stable cyclic form compared to the linear one.

Conclusions

The proposed chemical structure of the *N*-alkyl TPD ion species following the loss of a single hydrogen atom was revealed during APPI-HRMS-CID-MS^n (n=3) experiments of the $[M–H]^+$ ion species. A hydrogen radical ($H^•$) abstraction from the alkyl side chain (e.g. hexyl, heptyl, octyl, 2-ethylhexyl, and nonyl) activated a rearrangement of the *N*-alkyl-TPD derivatives radical cation structure initiating a cyclization and forming a six-membered ring that links the oxygen atom to the 3rd carbon atom in the alkyl chain. In addition, the theoretical calculations supported the APPI-HR-CID-MS^n (n=3) experiments by revealing that the proposed chemical structure resulted from the intramolecular cyclization of the *N*-alkyl-TPD ion species was stable in the presence of chlorobenzene. These research results will facilitate structural determination and elucidation of molecules with similar basic structures.

1 INTRODUCTION

The formation of positively charged species $[M–H]^+$ which resulted from the removal of a single hydrogen atom from the precursor molecules has been reported with a wide range of compounds using various ionization techniques.[1–6] This phenomenon is also common for alkanes.[7–10] Moreover, the $[M–H]^+$ species were pinpointed for different compound classes such as active pharmaceutical ingredients during LDI/MALDI-MS[1], hydroxy-4-phenyl-1,-2-dihydroquinoline derivatives during MALDI-TOF-MS,[2,3] benzoxazine monomers during MALDI-LTQ-Orbitrap-MS,[4] hydrocarbon analytes during nAPCI,[5] and alkaloids using multimatrix variation matrix-assisted laser desorption/ionization mass spectrometry (MALDI-MS)[11]. Hence, the mechanism formation of the $[M–H]^+$ ions by mass spectrometry in positive mode was previously reported in multiple studies.[6,12–16] In fact, three hypothesized mechanisms for generating $[M−H]^+$ were proposed. The first mechanism is a protonation followed by a loss of a hydrogen molecule (H_2) located on the alkyl side chain, the second possibility requires the formation of the $[M]^{+•}$ ion followed by an abstraction of a hydrogen radical ($H^•$), and the third mechanism is a direct abstraction of a hydride ($H^–$) from the [M] neutral molecule.

During our previous work, we investigated the formation of unusual $[M-H]^+$ ions during atmospheric pressure photoionization high-resolution mass spectrometry with chlorobenzene as a dopant,[16] from a class of *N*-alkyl-substituted thieno[3,4-c]pyrrole-4,6-dione (TPD) derivatives that are essential in the fabrication of photovoltaic polymer-based solar cells.[17–21] The compound dibromothieno[3,4-c]pyrrole-4,6-dione (TPD), with a nominal mass of 308 Da and the molecular formula $C_6H^{79}Br_2NO_2{}^{32}S$, exhibits enhanced electron-accepting capabilities when copolymerized with electron-donor monomers, such as dithiophene units, in donor-acceptor (D-A) alternating copolymers.[22–24] TPD has attracted significant research interest due to its straightforward synthesis, which can be achieved in a few steps from inexpensive, commercially available starting materials.[17,25] Studies have shown that the presence of linear or branched alkyl side chains on the TPD unit impacts the efficiency of solar cells. A key challenge in optimizing solar cell performance is the precise control over the number of aliphatic carbons in linear *N*-alkyl-substituted TPD derivatives.[18,19,21,26]

Specifically, the studied molecules shown in Scheme 1 contain different linear alkyl side chains (methyl, ethyl, butyl, hexyl, heptyl, octyl, 2-ethylhexyl, and nonyl) appended at the imide site. As a result of the previous investigation, *N*-methyl and *N*-ethyl-TPD derivatives favored the generation of $[M+H]^+$ ions with fewer $[M–H]^+$ ions. In contrast, *N*-butyl, *N*-hexyl, *N*-heptyl, *N*-octyl, *N*-2-ethylhexyl, and *N*-nonyl-TPD derivatives favored the generation of $[M–H]^+$ ions. The ion species $[M–H]^+$ were only observed under chlorobenzene-assisted photoionization conditions and in the presence of *N*-alkyl long-side chains, C_nH_{2n+1}, with $n \geq 4$ (**Figure S1**).[16] Furthermore, in the previous study, the CID-MS^n (n=2) experiments did not provide conclusive results for determining the final chemical structure of the *N*-alkyl-TPD species that have undergone hydrogen atom removal. On the other hand, density functional theory (DFT) simulations showed that the

formation of the $[M–H]^+$ ion is more likely to occur through the removal of a hydrogen molecule from the $[M+H]^+$ ion, leading to the formation of a C=C bond in the alkyl side chain.[16]

Since it is important to investigate the appropriate final chemical structure of the mentioned ion species of the studied substance, this discovery excluded the gas-phase intramolecular cyclization of *N*-alkyl-TPD molecules that resulted from the loss of the hydrogen radical $H^{\bullet}$ followed by the formation of potentially more stable cation species.

In this study, gas-phase fragmentation studies were performed to elucidate the structure of the $[M–H]^+$ ion formation in *N*-alkyl-substituted TPD derivatives photoionized at ambient pressure using higher-order MS^n high-resolution mass spectrometry (APPI-HR-CID-MS^n (n=3)). DFT calculations were performed to predict and analyze the structure of *N*-alkyl-TPD ion species, providing insights into their electronic properties and stability.

2 MATERIALS AND METHODS

2.1 Reagents

A fluoranthene standard at a concentration of 500 ng/mL in methanol was purchased from Restek Corporation (Bellefonte, PA, USA). Water was purified by a Milli-Q water purification system (Millipore, Milford, MA, USA). Methanol, acetonitrile, dichloromethane, and formic acid (LC/MS grade) were purchased from Thermo Fisher Scientific (Waltham, MA, USA). Chlorobenzene (>99.5%), was purchased from Acros Organics (Morris Plains, NJ, USA).

2.2 Preparation of *N*-alkyl derivatives

The five *N*-alkyl-substituted thieno[3,4-c]pyrrole-4,6-diones (*N*-TPDs) used in this study and described in **Scheme 1** were synthesized according to a previously reported method.[27]

The *N*-TPD derivatives sample preparation for high-resolution mass spectrometry was reported in the previous study.[16]

2.3 Ion sources and mass spectrometer

The analyses of the *N*-alkyl-substituted TPD derivatives (**Scheme 1**) were performed using a Thermo LTQ Velos Orbitrap mass spectrometer (ThermoFisher Scientific, Pittsburgh, PA, USA) equipped with different atmospheric pressure sources (Ion Max APCI, Syagen's Photo-Mate APPI) as described in the previous study. Collision-induced dissociation (CID) experiments were performed in the ion trap using 20–30% normalized collision energy (NCE). Activation parameter q was set to 0.25 and an activation time of 30 ms was applied. All higher-order MS/MS^n (n=3) spectra were acquired in the Orbitrap at a resolving power of 100 000 FWHM (full width at half maximum).

The source vaporizer temperature, sheath gas, auxiliary gas, dopant flow rate, discharge current, and the position of the APPI krypton lamp were optimized using a single PAH fluoranthene standard solution of 2.5 ng/µl (**Figure S2**). The capillary temperature was kept constant at 250 ˚C for all experiments. The source vaporizer temperature was adjusted to 450 ˚C **(Figure S2(a))**. Sheath and auxiliary gases were optimized and set to 60 and 30 arbitrary units, respectively. **(Figure S2(b))** The APCI discharge current was studied and showed to decrease the signal intensity (**Figure S2(d))**. The discharge current was turned off and set to zero in all experiments. The position of the APPI krypton lamp at the entrance of the mass spectrometer was adjusted to maximize the signal intensity of the $[M]^{+\bullet}$ ion of the PAH analyte. The chlorobenzene dopant solvent was delivered using the syringe pump (Thermo Fisher Scientific, Pittsburgh, PA, USA) and was combined with the LC eluent solvent after the separation and before entering the ion source using a zero dead volume-mixing tee. The dopant flow rate was optimized and set to 10% of the mobile phase flow rate. **(Figure S2(c))**.

2.4 Density functional theory calculations

To gain a deeper understanding of the mechanism behind the formation of the $[M–H]^+$ ions possibly involving an intramolecular cyclization structure of the studied *N*-alkyl-TPD species, two TPD derivatives with the *N*-alkyl side chain C_nH_{2n+1} (n = 6 & n=9) were modelized with DFT. Geometry optimization, frequency and single point energy calculations were obtained in the gas phase (T = 298.15 K) using the B3LYP functional [28,29] associated to the 6-311++G(d,p) basis set [30,31]. The trustworthiness of B3LYP/6-311+(d,p) has been confirmed by earlier reports [32–36]. All calculations were carried out using the Gaussian16 (Rev.C.02) package.[37]

3 RESULTS AND DISCUSSION

As reported in the previous study, under APPI conditions using chlorobenzene as the dopant, CID-MS/MS fragmentation of $[M_{1\text{-}5}–H]^+$ ions generated from the five studied *N*-alkyl-substituted TPD derivatives (**Figure S3**) exhibited a specific fragmentation pattern compared to the MS/MS fragmentation of $[M_{1\text{-}5}+H]^+$ ions generated from the same molecules under ESI and APCI conditions.[16] The product ions of each studied molecule during the APPI MS/MS experiment of the $[M_{1\text{-}5}–H]^+$ ions were observed to be associated with the loss of a water molecule (18 Da), as well as product ions differing by 14 Da. Additionally, two common TPD fragment ions were detected at *m/z* 310 and *m/z* 322. As a result, these APPI-CID-HR-MS/MS experimental outcomes are not sufficient to confirm a conclusive final chemical structure molecules identity of the observed $[M_{1\text{-}5}–H]^+$ ion species.

Furthermore, as reported in the previous study, under APPI conditions with chlorobenzene as the dopant, TPD derivatives with the *N*-alkyl side chain C_nH_{2n+1} (n ≥4) generally promoted the formation of $[M–H]^+$ ions. As demonstrated in Figure S1(c)&(d), TPD-C_nH_{2n+1} (n=4 and n=6) produce a stable precursor $[M–H]^+$ at *m/z* 364 and *m/z* 392 respectively with the disappearance of

the $[M+H]^+$ ions species. In contrast, when TPD-C_nH_{2n+1} (n=1 and n=2), the stable precursor $[M+H]^+$ ions at *m/z* 324 and *m/z* 338 are more favored despite the presence of $[M–H]^+$ ions species as shown in Figure S1(b).

In this study, we propose that the chemical structure of the predominant $[M–H]^+$ ion species results from the elimination of a single hydrogen atom, leading to the formation of a six-membered cyclic system. In this configuration, the oxygen atom is bonded to the third carbon atom (C-3), leading to enhanced stability in the gas phase (**Scheme 2(a)**).

Similarly, we propose that the chemical structure of the less abundant $[M–H]^+$ ion species results from the elimination of a single hydrogen atom, leading to the formation of a five-membered cyclic system. In this configuration, the oxygen atom is bonded to the third carbon atom (C-3), leading to reduced stability in the gas phase (**Scheme 2(b)**).

As a result, our innovative exploration proposes that the chemical structure of the $[M_{1\text{-}5}–H]^+$ ions for the studied molecules is formed through the loss of a hydrogen radical ($H^{\bullet}$), followed by a structural rearrangement that generates 1,6-cyclized *N*-alkyl-TPD ion species, as illustrated in Scheme 3 and Scheme S1. It is important to note that the specific transfer of the hydrogen atom can only be confirmed using a suitably deuterium-labeled compound. Therefore, conducting additional experiments, such as collision-induced dissociation mass spectrometry (CID-MS^n, where n=3) and electronic structure calculations, will help to support the proposed mechanism of the formation of these ion species.

3.1 APPI-CID-HR-MS^n (n=3) investigation of the $[M–H]^+$ ions generated from the *N*-alkyl-substituted TPD derivatives

In the CID-MS/MS experiment shown in Figure 1(a), the ion $[C_{12}H_{12}{}^{79}Br_2NO_2{}^{32}S]^+$ at *m/z* 391.89575 generates the ion $[C_7H_2{}^{79}Br_2NO_2{}^{32}S]^+$ at *m/z* 321.81731 through the loss of a pentene molecule (C_5H_{10}, 70 Da) via a retro-Diels-Alder mechanism.[38] (**Scheme 4**)

Additionally, Figure 1(a) shows the product ion $[C_6H_2{}^{79}Br_2NO^{32}S]^+$ at *m/z* 309.81743, potentially formed by the loss of a 1,3 hexadiene molecule (C_6H_{10}, 82 Da). This loss may occur through an ion-dipole complex resulting from the rearrangement of the 1,6 cyclization *N*-hexyl-TPD derivative $[M_1–H]^+$ ion at *m/z* 392 (**Scheme S2**). Furthermore, Figure 1(a) also shows the product ion $[C_9H_6{}^{79}Br_2NO^{32}S]^+$ at *m/z* 349.84867, likely formed through the unusual loss of a propene molecule (C_3H_6, 42 Da), possibly via an ion-molecule complex involving allyl cation.

To further investigate the structure of the $[M_{1\text{-}5}–H]^+$ species, (CID-MS^n (n=3)) experiments were conducted on select product ions, including those at *m/z* 350, 336, and 322, generated during the CID-MS/MS analysis of the *N*-hexyl-TPD derivative 1.

The CID-MS/MS/MS experiment presented in Figure 1(b) shows that the ion $[C_9H_6{}^{79}Br_2NO^{32}S]^+$ at *m/z* 349.84862 forms the ion $[C_7H_2{}^{79}Br_2NO^{32}S]^+$ at *m/z* 321.81731 through the loss of ethene molecule (C_2H_4, 28 Da) through a retro-Diels-Alder mechanism.[38] (**Scheme 4**)

Additionally, the CID-MS/MS/MS fragmentation of the ion $[C_9H_6{}^{79}Br_2NO_2{}^{32}S]^+$ at *m/z* 349.84862 produces the ion $[C_6H_2{}^{79}Br_2NO^{32}S]^+$ at *m/z* 309.81726. (**Figure 1(b)**)

Hence, the CID-MS/MS/MS experiment shown in Figure 1(c) of the ion $[C_8H_4{}^{79}Br_2NO_2{}^{32}S]^+$ at *m/z* 335.83292 produces the ion at *m/z* 308.82196.

Finally, the CID-MS/MS/MS of the ion $[C_7H_2{}^{79}Br_2NO_2{}^{32}S]^+$ at *m/z* 321.81729 shown in Figure 1(d) produces the ion $[C_6H^{79}Br_2O_2{}^{32}S]^+$ at *m/z* 294.80589 from the loss of the neutral molecule (CHN, 27 Da). (**Scheme 4**)

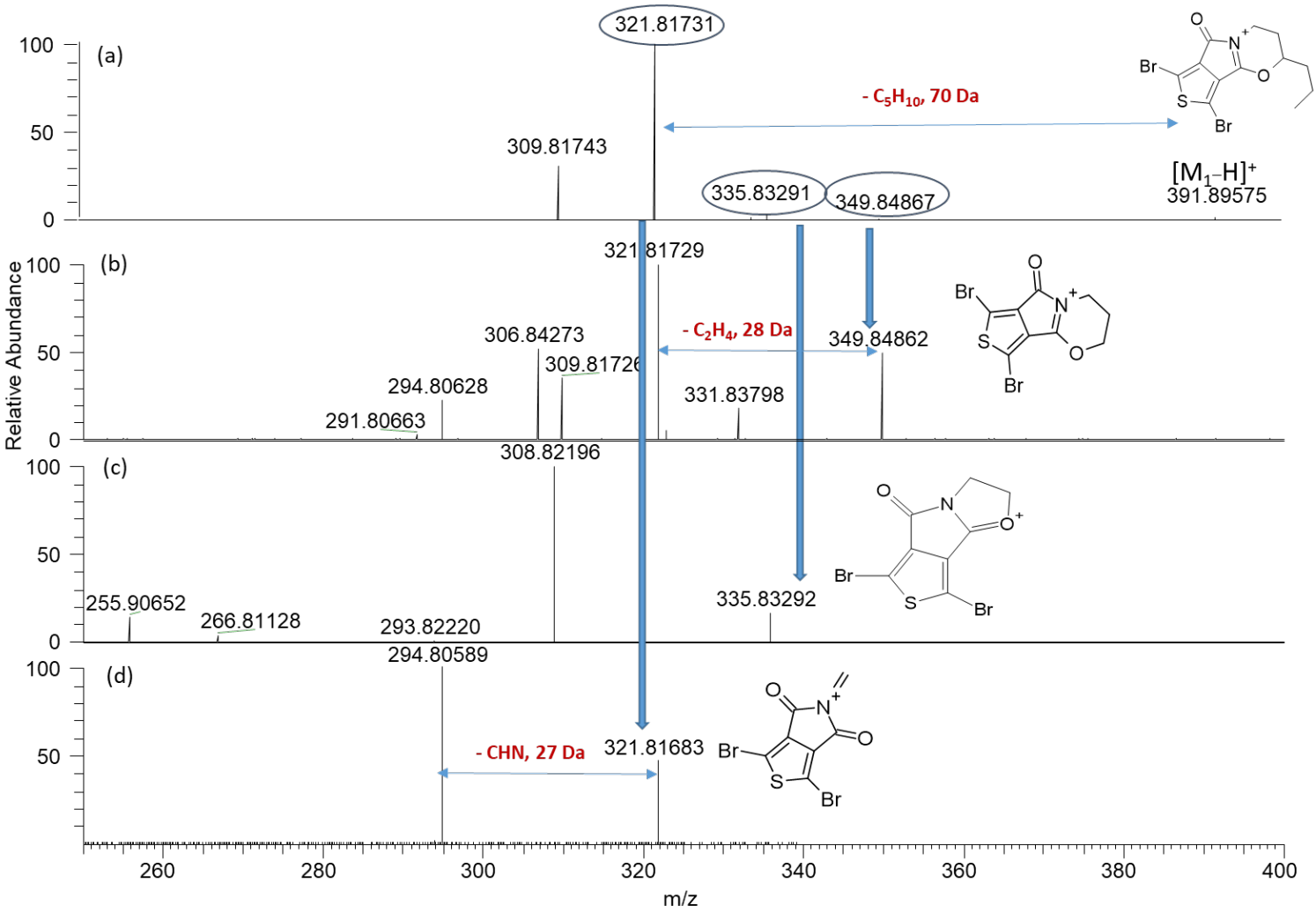

Figure 1. (a) the APPI-(+)-CID-MS/MS (NCE= 20%) spectrum of the precursor ion *N*-hexyl TPD derivative 1 $[M_1–H]^+$ ion at *m/z* 392, (b) the APPI-(+)-CID-MS/MS/MS (NCE=20%) spectrum of the product-ion at *m/z* 350, (c) the APPI-(+)-CID-MS/MS/MS (NCE: 20%) spectrum of the product-ion at *m/z* 336, (d) the APPI-(+)-CID-MS/MS/MS (NCE= 20%) spectrum of the product-ion at *m/z* 322.

Similar fragmentation routes were observed for the rest of the studied TPD derivative ion species. For example, the CID-MS/MS/MS of some product ions generated from the rearranged 1,6 cyclized *N*-nonane-TPD derivative ion $[M_5–H]^+$ such as at *m/z* 392, 378, and 364, are shown in the supplementary material (**Figure S4**). A retro-Diels-Alder fragmentation mechanism was observed in all studied molecules, leading to the formation of a common fragment ion at *m/z* 322, which supports the structure rearrangement of the *N*-alkyl-TPD derivatives.

Following the structural insights gained, computational experiments were further employed to support the proposed structure of the $[M_{1\text{-}5}–H]^+$ ion in the studied *N*-alkyl-TPD derivatives.

3.2 Computational analysis of the formation of $[M_{1\&5}–H]^+$ ion formation in the 1-6 cyclized *N*-Alkyl-TPD ion species.

When one H atom is removed from the *N*-alkyl side chain of the TPD molecules, the system energy is expected to become higher due to the generation of the hydrogen radical ($H^{\bullet}$). This is confirmed by our calculations for both *N*-alkyl-TPD1 and *N*-alkyl-TPD5. The thermodynamically most favored localization for removal of $H^{\bullet}$ appears to be on C3 of the *N*-alkyl side chain and can either lead to a cyclic or a linear structure. Both were probed and the cyclic structure was shown to be the most stable one, located 26.5 and 27.9 kcal/mol above the corresponding *N*-alkyl-TPD1 and *N*-alkyl-TPD5 molecular ions, respectiveley. Linear forms of these two fragments ions are more than 10 kcal/mol higher in energy than cyclic ones for both TPD1 and TPD5 (Figure 2).

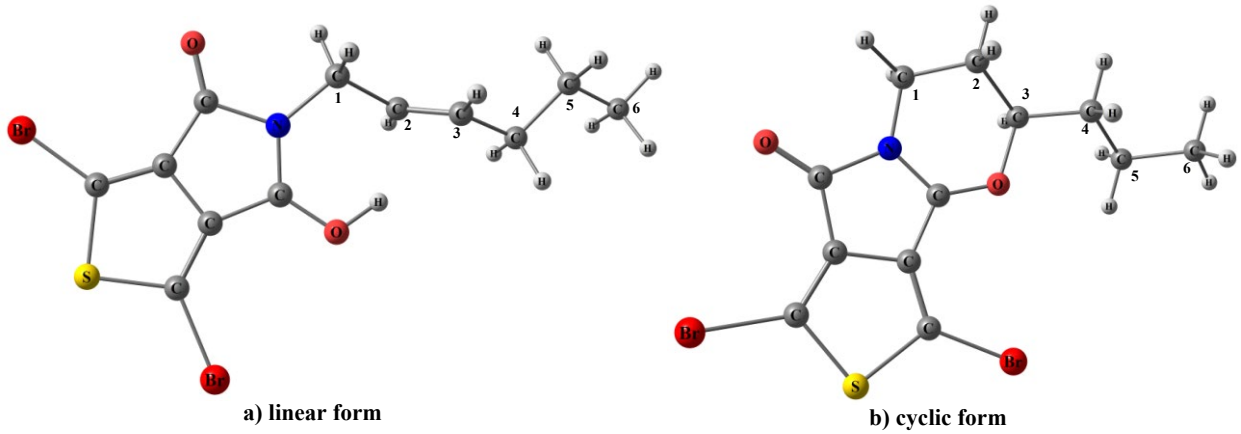

Figure 2. Optimized (a) linear and (b) cyclic geometries of the $[M–H]^+$ ions of a TPD1 derivative with the *N*-alkyl side chain C_nH_{2n+1} (n = 6). The cyclic geometry is 11.3 kcal/mol more stable than the linear one.

The introduction of the chlorobenzene molecule (C_6H_5Cl) to the system may promote the elimination of the generated $H^•$ radical. Formation of the TPD1 $[M–H]^+$ ion through the reaction of the $M^{+•}$ precursor with C_6H_5Cl and leading to C_6H_6 and $Cl^•$ helps lowering the energetic cost of the reaction as the endothermicity drops by 20.2 kcal/mol to reach a fragment only 6.3 kcal/mol above the precursor ion (see Table S1). Although the full reaction energy pathway was not completely defined, particularly the transition structures, which would offer deeper insights into the reaction profile, this still provides valuable understanding about the role played by the chlorobenzene molecule to favored the reaction..

4 CONCLUSION

The APPI-HRMS-CID-MS/MS/MS investigations presented in this work elucidated the chemical structure of the *N*-alkyl TPD ion species $[M_{1\text{-}5}–H]^+$, following the loss of a single hydrogen atom. The proposed 1,6 cyclization of *N*-alkyl TPD ions occurs after the abstraction of the hydrogen radical ($H^•$), initiating the cyclization and forming a six-membered ring that links the oxygen atom

to the third carbon atom in the alkyl side chain. A reversed-Diels-Alder fragmentation mechanism, leading to a common fragment ion at *m/z* 322, further corroborated the structural rearrangement of the 1,6 cyclized *N*-alkyl-TPD derivatives as DFT calculations.

As a result, the current work demonstrated that APPI-HR-CID-MS/MS^n experiments are crucial for detecting some gas-phase fragmentation patterns of ionized species, and computational approaches are an effective tool for understanding these processes driving advancements in chemical analysis and compound identification.

5 ACKNOWLEDGEMENTS

The research reported here was supported by King Abdullah University of Science and Technology. In addition, the authors gratefully acknowledge Dr. Patricia Lopez Sanchez and research support from the Analytical Core Lab of King Abdullah University of Science and Technology, Saudi Arabia. Some of the simulations were conducted on the SACADO MeSU platform at Sorbonne University, with their support gratefully acknowledged.

6 REFERENCES

1. Bronzel, J. L., Milagre, C. D. F. & Milagre, H. M. S. Analysis of low molecular weight compounds using MALDI- and LDI-TOF-MS: Direct detection of active pharmaceutical ingredients in different formulations. *J Mass Spectrom* **52**, 752–758 (2017).
2. Tabassum, R., Ashfaq, M. & Oku, H. 7-Hydroxy-4-phenyl-1, 2-dihydroquinoline derivatives: synthesis via one-pot, three-component reaction and structure elucidation. *Heliyon* **6**, e05035 (2020).
3. Tabassum, R., Ashfaq, M. & Oku, H. Development of an efficient, one-pot, multicomponent protocol for synthesis of 8-hydroxy-4-phenyl-1,2-dihydroquinoline derivatives. *J Heterocycl Chem* **58**, 534–547 (2021).
4. Puchot, L. *et al.* Breaking the symmetry of dibenzoxazines: A paradigm to tailor the design of bio-based thermosets. *Green Chem* **18**, 3346–3353 (2016).
5. Kulyk, D. S., Sahraeian, T., Wan, Q. & Badu-Tawiah, A. K. Reactive Olfaction Ambient Mass Spectrometry. *Anal Chem* **91**, 6790–6799 (2019).
6. Gao, Y. *et al.* Ambient electric arc ionization for versatile sample analysis using mass spectrometry. *Analyst* **146**, 5682–5690 (2021).
7. Marotta, E. & Paradisi, C. A Mass Spectrometry Study of Alkanes in Air Plasma at Atmospheric Pressure. *J. Am. Soc. Mass Spectrom* **20**, 697–707 (2009).
8. Gao, J., Owen, B. C., Borton, D. J., Jin, Z. & Kenttämaa, H. I. *HPLC/APCI mass s*pectrometry of saturated and unsaturated hydrocarbons by using hydrocarbon solvents as the APCI reagent and HPLC mobile phase. *J. Am. Soc. Mass Spectrom* **23**, 816–822 (2012).
9. Cody, R. B. Observation of Molecular Ions and Analysis of Nonpolar Compounds with

the Direct Analysis in Real Time Ion Source. *Anal. Chem* **81**, 1101–1107 (2009).

10. Suni, N. M., Aalto, H., Kauppila, T. J., Kotiaho, T. & Kostiainen, R. Analysis of lipids with desorption atmospheric pressure photoionization-mass spectrometry (DAPPI-MS) and desorption electrospray ionization-mass spectrometry (DESI-MS). *J. Mass Spectrom* **47**, 611–619 (2012).
11. Yamagaki, T., Osawa, T., Fujikawa, K., Watanabe, T. & Sugahara, K. Multimatrix Variation Matrix-Assisted Laser Desorption/Ionization Mass Spectrometry as a Tool for Determining the Bonding of Nitrogen Atoms in Alkaloids. *J Am Soc Mass Spectrom* **33**, 2243–2249 (2022).
12. Awad, H. *et al.* The unexpected formation of [M - H]+ species during MALDI and dopant-free APPI MS analysis of novel antineoplastic curcumin analogues. *J Mass Spectrom* **49**, 1139–1147 (2014).
13. Kang, C. *et al.* Dehydrogenation and dehalogenation of amines in MALDI-TOF MS investigated by isotopic labeling. *J Mass Spectrom* **48**, 1318–1324 (2013).
14. Matsuta, S. *et al.* Dehydration-fragmentation mechanism of cathinones and their metabolites in ESI-CID. *J Mass Spectrom* **55**, (2020).
15. Lou, X. W. *et al.* Dehydrogenation of tertiary amines in matrix-assisted laser desorption/ionization time-of-flight mass spectrometry. *J Mass Spectrom* **43**, 1110–1122 (2008).
16. Sioud, S. *et al.* The formation of [M-H] + ions in N -alkyl-substituted thieno[3,4- c]-pyrrole-4,6-dione derivatives during atmospheric pressure photoionization mass spectrometry. *Rapid Commun Mass Spectrom* **28**, 2389–2397 (2014).
17. Cabanetos, C. *et al.* Linear side chains in benzo[1,2-b:4,5-b′]dithiophene-thieno[3,4-c]

pyrrole-4,6-dione polymers direct self-assembly and solar cell performance. *J. Am. Chem. Soc* **135**, 4656–4659 (2013).

18. Schultes, S. M., Sullivan, P., Heutz, S., Sanderson, B. M. & Jones, T. S. The role of molecular architecture and layer composition on the properties and performance of CuPc-C60 photovoltaic devices. *Mater. Sci. Eng. C* **25**, 858–865 (2005).

19. Kroon, R., Lenes, M., Hummelen, J. C., Blom, P. W. M. & De Boer, B. Small bandgap polymers for organic solar cells (polymer material development in the last 5 years). *Polym. Rev* **48**, 531–582 (2008).

20. Q. Li et al. The alkyl chain positioning of thieno[3,4-c]pyrrole-4,6-dione (TPD)-Based polymer donors mediates the energy loss, charge transport, and recombination in polymer solar cells. *J Power Sources* **480**, 229098 (2020).

21. Pandey, L., Risko, C., Norton, J. E. & Brédas, J. L. Donor-acceptor copolymers of relevance for organic photovoltaics: A theoretical investigation of the impact of chemical structure modifications on the electronic and optical properties. *Macromolecules* **45**, 6405–6414 (2012).

22. Lin, Z., Bjorgaard, J., Gul Yavuz, A., Iyer, A. & Köse, M. E. Synthesis, photophysics, and photovoltaic properties of low-bandgap conjugated polymers based on thieno[3,4-c]pyrrole-4,6-dione: a combined experimental and computational study. *RSC Adv.* **2**, 642–651 (2012).

23. Najari, A. *et al. S*ynthesis and characterization of new thieno[3,4-c]pyrrole-4,6-dione derivatives for photovoltaic applications. *Adv. Funct. Mater* **21**, 718–728 (2011).

24. Zou, Y. *et al. A* Thieno[3, 4-c]pyrrole-4, 6-dione-Based Copolymer for Efficient Solar Cells. *J. Am. Chem. Soc* **132**, 5330–5331 (2010).

25. Beaupré, S. *et al.* Thieno-, furo-, and selenopheno[3,4-c]pyrrole-4,6-dione copolymers: Effect of the heteroatom on the electrooptical properties. *Macromolecules* **45**, 6906–6914 (2012).

26. Mühlbacher, D. *et al.* High photovoltaic performance of a low-bandgap polymer. *Adv. Mater***18**, 2884–2889 (2006).

27. Berrouard, P., Dufresne, S., Pron, A., Veilleux, J. & Leclerc, M. Low-cost synthesis and physical characterization of thieno[3,4-c]pyrrole-4,6-dione-based polymers. *J Org Chem* **77**, 8167–73 (2012).

28. Becke, A. D. Density-functional exchange-energy approximation with correct asymptotic behavior. *Phys Rev A* **38**, 3098–3100 (1988).

29. Lee C., Yang W., P. R. . Development of the Colle-Salvetti correlation-energy formula into a functional of the electron density. *Phys Rev B* **37**, 785–789 (1988).

30. López-López, J. A. *et al.* Contracted Gaussian basis sets for molecular calculations. *J Chem Phys* **72**, 970–982 (1980).

31. Krishnan R., Binkley J.S., Seeger R., P. J. . Self-consistent molecular orbital methods. XX. A basis set for correlated wave functions. *J Chem Phys* **72**, 650–654 (1980).

32. Tirado-Rives J., J. W. . Performance of B3LYP Density Functional Methods for a Large Set of Organic Molecules. *J Chem Theory Comput* **4**, 397–306 (2008).

33. Coskun D., Jerome S.V., F. R. . Evaluation of the Performance of the B3LYP, PBE0, and M06 DFT Functionals, and DBLOC-Corrected Versions, in the Calculation of Redox Potentials and Spin Splittings for Transition Metal Containing Systems. *J Chem Theory Comput* 1121–1128 (2016).

34. Lopez-Lopez J.A., A. R. Assessment of the performance of commonly used DFT

functionals vs. MP2 in the study of IL-Water, IL-Ethanol, and IL-(H2O)3 clusters. *J Mol Liq* **220**, 970–982 (2016).

35. Kumar N., Goel N., Yadav T.C., P. V. Quantum chemical, ADMET and molecular docking studies of ferulic acid amide derivatives with a novel anticancer drug target. *Med Chem Res* **26**, 1822–1834 (2017).

36. Lai W.-J., Lu J.-H., Jiang L.-H., Lei F.-H., Shen L.-Q., Wu A.-Q., Yang J., Q. W.-L. Structural stabilities and transformation mechanism of rhynchophylline and isorhynchophylline in aqueous and methanol solution based on high-performance liquid chromatography and density functional theory. *J Mol Struct* **1236**, (2021).

37. Frisch M.J., Trucks G.W., Schlegel H.B., Scuseria G.E., Robb M.A., Cheeseman J.R., S. G. & Barone V., Petersson G.A., Nakatsuji H., et a. Gaussian 16. *, Revis C02 Gaussian, Inc* (2016).

38. Tureček, F. *et al.* Retro-Diels-Alder reaction in mass spectrometry. *Mass Spectrom Rev* **95**, 85–152 (1973).